Zinelaabidine BOUDJEMA[1], Abdelkader MEROUFEL[2], Ahmed AMARI[3]

Intelligent Control & Electrical Power Systems Laboratory, Faculty of Engineer Science, Electrical Engineering Department, University of Djillali Liabes, BP 98 Sidi Bel-Abbès 22000 Algeria (1,2), Electrical Engineering Department, University of Mostaganem, Algeria (3).

Robust Control of a Doubly Fed Induction Generator (DFIG) Fed by a Direct AC-AC Converter

Abstract. The aim of this paper is to propose a robust control method for a doubly-fed induction generator fed by a direct AC-AC converter used in wind energy conversion systems. First, we carried out a study of modelling on the matrix converter controlled by the venturini modulation technique. Thereafter, stator active and reactive powers are regulated by controlling the machine inverter with two different controllers : proportional–integral and Sliding mode. Simulations results are presented and discussed for the whole system.

Streszczenie. W artykule opisano metodę sterowania dla generatora indukcyjnego o zasilaniu dwustronnym z przekształtnika matrycowego (AC-AC) w aplikacji do turbiny wiatrowej. Przedstawiono model przekształtnika matrycowego o modulacji metodą venturini oraz wyniki badań symulacyjnych. (Sterowanie o zwiększonej odporności dla generatora indukcyjnego o zasilaniu dwustronnym, zasilanego przekształtnikiem matrycowym)

Keywords : Doubly fed induction generator, Matrix converter, PI controller, Sliding mode controller.
Słowa kluczowe: Generator indukcyjny o zasilaniu dwustronnym, przekształtnik matrycowy, regulator PI, regulator ślizgowy.

Introduction

Wind energy is the most promising renewable source of electrical power generation for the future. Many countries promote the wind power technology through various national programs and market incentives. Wind energy technology has evolved rapidly over the past three decades with increasing rotor diameters and the use of sophisticated power electronics to allow operation at variable speed [1]. Doubly fed induction generator is one of the most popular variable speed wind turbines in use nowadays. It is normally fed by a voltage source inverter. However, nowadays the matrix converter is popular in the market due to a number of advantages, such as sinusoidal input and output waveforms, bi-directional energy flow capability, controllable input displacement factor, and high power/volume ratio because of the absence of a DC link filter [2, 3]. Consequently, in this work, a three-phase matrix converter is used to drive the doubly fed induction generator.

In recent years, dozens of work was done by researchers on the control of DFIG using a simplified model of the latter by negligence the stator resistance. This assumption, although it has been proven that it is a realistic approximation for medium power machines used in wind energy conversion, but in reality, the model does not reflect reality because this parameter still exists and it can not be neglected. To overcome this drawback, in this work and in contrast to previous work, we used a real model of DFIG, ie without negligence in this resistance.

Many papers have been presented with different control schemes of DFIG. These control schemes are generally based on vector control concept with classical PI controllers as proposed by Pena et al. in [4] and Poller in [5]. The same classical controllers are also used to achieve control techniques of DFIG when grid faults appear like unbalanced voltages [6,7] and voltage dips [8]. It has also been shown in [9,10] that flicker problems could be solved with appropriate control strategies. Many of these studies confirm that stator reactive power control can be an adapted solution to these different problems.

This paper presents a control method for the machine inverter in order to regulate the active and reactive power exchanged between the machine and the grid. The active power is controlled in order to be adapted to the wind speed in a wind energy conversion system and the reactive power control allows to get a unitary power factor between the stator and the grid. Such an approach does not manage easily the compromise between dynamic performances and

robustness or between dynamic performances and the generator energy cost. These compromises cannot easily be respected with classical PI controllers proposed in most DFIG control schemes. Moreover, if the controllers have bad performances in systems with DFIG such as wind energy conversion, the quality and the quantity of the generated power can be affected. It is then proposed to study the behaviour of a Sliding Mode Controller (SMC). The two controllers are compared and results are discussed, the objective is to show that SMC controllers can improve performances of doubly-fed induction generators in terms of reference tracking, sensibility to perturbations and parameters variations.

Matrix converter model :

The matrix converter is an alternative to an inverter drive for three-phase frequency control. The converter consists of nine bi-directional switches arranged into three sets of three, so that any of the three input phases can be connected to any of the three output lines, as shown in figure 1, where uppercase and lowercase letters are used to denote the input and output, respectively. The switches are then controlled in such a way that the average output voltages are a three-phase set of sinusoids of the required frequency and magnitude [2].
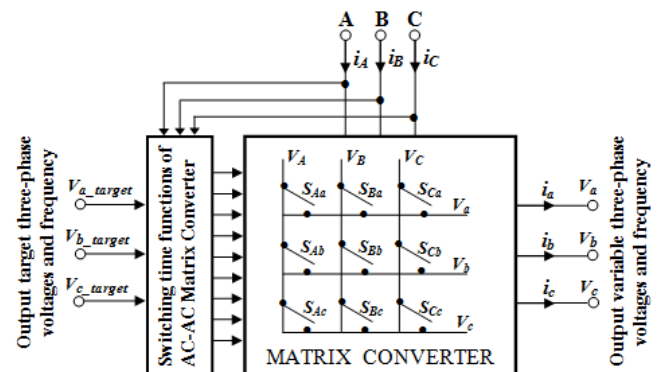
Fig. 1. Schematic representation of the matrix converter.

The matrix converter can comply with four quadrants of motor operations, while generating no higher harmonics in the three-phase AC power supply. Compared to conventional drives, there is potential for reduced cost of manufacture and maintenance, and increased power/weight and power/volume ratios. The circuit is inherently capable of

bi-directional power flow, and also offers virtually sinusoidal input current, without the harmonics usually associated with present commercial inverters [7].

The switching function of a switch S_{ij} in figure 1 is defined as :

$$(1) \qquad S_{ij} = \begin{cases} 1 & S_{ij} \text{ is closed} \\ 0 & S_{ij} \text{ is open} \end{cases} \quad i \in \{a,b,c\}, \; j \in \{A,B,C\}$$

The switching angles formulation :

The switching angles, of the nine bidirectional switches S_{ij} witch will be calculated, must comply with the following rules :

►At any time 't', only one switch S_{ij} (j=1, 2, 3) will be in 'ON' state. This assures that no short circuit will occur at the input terminals,

►At any time 't', at least two of the switches S_{ij} (i=1, 2, 3) will be in 'ON' state. This condition guarantees a closed-loop path for the load current (usually this is an inductive current).

During the kth switching cycle T_s (T_s=$1/f_s$) (Fig.2), the first phase output voltage is given by :

$$(2) \qquad V_a = \begin{cases} V_A & 0 \le t\text{-}(k\text{-}1)T_s < m_{aA}^k T_s \\ V_B & m_{aA}^k T_s \le t-(k\text{-}1)T_s < \left(m_{aA}^k + m_{aB}^k \right)T_s \\ V_C & \left(m_{aA}^k + m_{aB}^k \right)T_s \le t\text{-}(k\text{-}1)T_s < T_s \end{cases}$$

where 'm's are defined by :

$$(3) \qquad m_{ij}^k = \frac{t_{ij}^k}{T_s}$$

where t_{ij}^k : Time interval when S_{ij} is in 'ON' state, during the kth cycle and k is being the switching cycle sequence number. The 'm's have the physical meaning of duty cycle. Also, $m_{iA}^k + m_{iA}^k + m_{iA}^k$ and $0 < m_{ij}^k < 1$. Which means that during every cycle T_s all switches will turn on and off once.

$$\underbrace{\begin{matrix} t_{aA}^{(1)} \; t_{aB}^{(1)} \; t_{aC}^{(1)} \\ \end{matrix}}_{t=0} \underbrace{\begin{matrix} t_{aA}^{(2)} \; t_{aB}^{(2)} \; t_{aC}^{(2)} \\ \end{matrix}}_{T_s} \; ------- \; \underbrace{\begin{matrix} t_{aA}^{(k)} \; t_{aB}^{(k)} \; t_{aC}^{(k)} \\ \end{matrix}}_{(k-1)T_s} \xrightarrow{\text{Time}}$$
$$t{=}0 \qquad T_s \qquad 2T_s \qquad \qquad (k\text{-}1)T_s \qquad kT_s$$
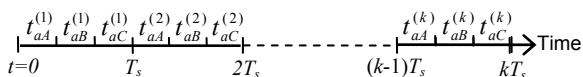
Fig. 2. Segmentation of the axis time for the consecutive orders of intervals closing of the switeches.

Algorithm of Ventirini :

The algorithm of Venturini (1980) and Alesina and Venturini (1988), allows a control of the S_{ij} switches so that the low frequency parts of the synthesized output voltages (V_a, V_b and V_c) and the input currents (i_{Ar}, i_{Br} and i_{Cr}) are purely sinusoidal with the prescribed values of the output frequency, the input frequency, the displacement factor and the input amplitude. The average values of the output voltages during the kth sequence are thus given by [12]:

$$(4) \qquad \begin{cases} V_a = \dfrac{t_{aA}^k}{T_s} V_A + \dfrac{t_{aB}^k}{T_s} V_B + \dfrac{t_{aC}^k}{T_s} V_C \\[2mm] V_b = \dfrac{t_{bA}^k}{T_s} V_A + \dfrac{t_{bB}^k}{T_s} V_B + \dfrac{t_{bC}^k}{T_s} V_C \\[2mm] V_c = \dfrac{t_{cA}^k}{T_s} V_A + \dfrac{t_{cB}^k}{T_s} V_B + \dfrac{t_{cC}^k}{T_s} V_C \end{cases}$$

If times of conduction are modulated in the shape of sinusoidal with the pulsation W_m while T_s remains constant, such as $w_0 w_i + w_m$ these times are defined as follows :

▪ For the 1st phase, we have :

$$(5) \qquad \begin{cases} t_{aA} = \dfrac{T_s}{3}\left(1+2\delta\cos\left(w_m t+\theta\right)\right) \\[3mm] t_{aA} = \dfrac{T_s}{3}\left(1+2\delta\cos\left(w_m t+\theta-\dfrac{2\pi}{3}\right)\right) \\[3mm] t_{aA} = \dfrac{T_s}{3}\left(1+2\delta\cos\left(w_m t+\theta-\dfrac{4\pi}{3}\right)\right) \end{cases}$$

▪ For the 2nd phase :

$$(6) \qquad \begin{cases} t_{bA} = \dfrac{T_s}{3}\left(1+2\delta\cos\left(w_m t+\theta-\dfrac{4\pi}{3}\right)\right) \\[3mm] t_{bB} = \dfrac{T_s}{3}\left(1+2\delta\cos\left(w_m t+\theta\right)\right) \\[3mm] t_{bC} = \dfrac{T_s}{3}\left(1+2\delta\cos\left(w_m t+\theta-\dfrac{2\pi}{3}\right)\right) \end{cases}$$

▪ For the 3rd phase :

$$(7) \qquad \begin{cases} t_{cA} = \dfrac{T_s}{3}\left(1+2\delta\cos\left(w_m t+\theta-\dfrac{2\pi}{3}\right)\right) \\[3mm] t_{cB} = \dfrac{T_s}{3}\left(1+2\delta\cos\left(w_m t+\theta-\dfrac{4\pi}{3}\right)\right) \\[3mm] t_{cC} = \dfrac{T_s}{3}\left(1+2\delta\cos\left(w_m t+\theta\right)\right) \end{cases}$$

Where θ is the initial phase angle. The output voltage is given by :

$$(8) \qquad \begin{bmatrix} v_a \\ v_b \\ v_c \end{bmatrix} = \begin{bmatrix} 1+2\delta\cos\alpha & 1+2\delta\cos\left(\alpha-\dfrac{2\pi}{3}\right) & 1+2\delta\cos\left(\alpha-\dfrac{4\pi}{3}\right) \\[3mm] 1+2\delta\cos\left(\alpha-\dfrac{4\pi}{3}\right) & 1+2\delta\cos\alpha & 1+2\delta\cos\left(\alpha-\dfrac{2\pi}{3}\right) \\[3mm] 1+2\delta\cos\left(\alpha-\dfrac{2\pi}{3}\right) & 1+2\delta\cos\left(\alpha-\dfrac{4\pi}{3}\right) & 1+2\delta\cos\alpha \end{bmatrix} \begin{bmatrix} V_A \\ V_B \\ V_C \end{bmatrix}$$

where : $\begin{cases} a = w_m + \theta \\ w_m = w_o - w_i \end{cases}$

The running matrix converter with Venturini algorithm generates at the output a three-phases sinusoidal voltages system having in that order pulsation w_m, a phase angle θ and amplitude $\delta.V_s$. ($0 < \delta < 0.866$ with modulation of the neural) (Venturini, 1980).

The DFIG model :

The application of Concordia and Park's transformation to the three-phase model of the DFIG permits to write the dynamic voltages and fluxes equations in an arbitrary d–q reference frame :

$$(9) \qquad \begin{cases} V_{ds} = R_s I_{ds} + \dfrac{d}{dt}\psi_{ds} - \omega_s\psi_{qs} \\[3mm] V_{qs} = R_s I_{qs} + \dfrac{d}{dt}\psi_{qs} + \omega_s\psi_{ds} \\[3mm] V_{dr} = R_r I_{dr} + \dfrac{d}{dt}\psi_{dr} - \omega_r\psi_{qr} \\[3mm] V_{qr} = R_r I_{qr} + \dfrac{d}{dt}\psi_{qr} + \omega_r\psi_{dr} \end{cases}$$

$$(10) \quad \begin{cases} \psi_{ds} = L_s I_{ds} + M I_{dr}, \ \psi_{qs} = L_s I_{qs} + M I_{qr} \\ \psi_{dr} = L_r I_{dr} + M I_{ds}, \ \psi_{qr} = L_r I_{qr} + M I_{qs} \end{cases}$$

The stator and rotor angular velocities are linked by the following relation : $\omega_s = \omega + \omega_r$.
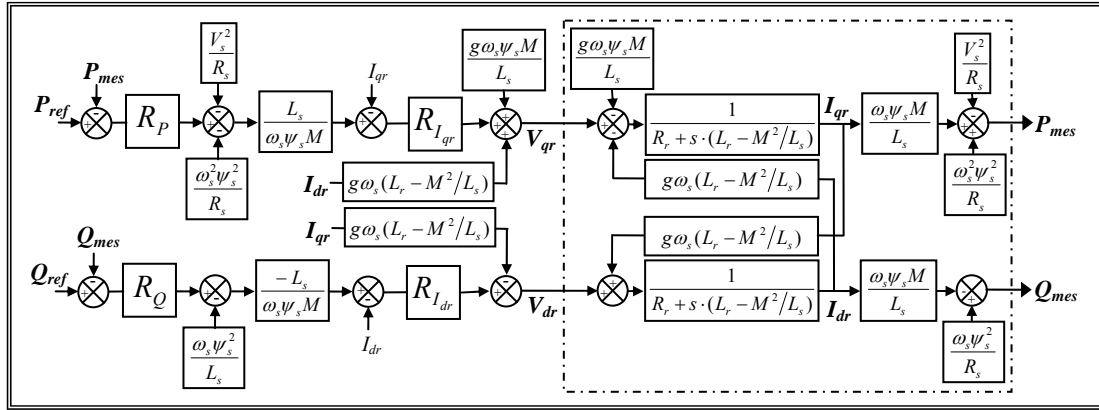
Fig. 3. Power control of DFIG.

This electrical model is completed by the mechanical equation :

$$(11) \quad C_{em} = C_r + J\frac{d\Omega}{dt} + f\Omega$$

Where the electromagnetic torque C_{em} can be written as a function of stator fluxes and rotor currents :

$$(12) \quad C_{em} = pp\frac{M}{L_s}\left(\psi_{qs}I_{dr} - \psi_{ds}I_{qr}\right)$$

DFIG field orientation strategy :
In order to easily control the production of electricity by the wind turbine, we will carry out an independent control of active and reactive powers by orientation of the stator flux. This orientation will be made in this work with a real model of the DFIG, i.e. without negligence of the stator resistance [13].

By choosing a reference frame linked to the stator flux, rotor currents will be related directly to the stator active and reactive power. An adapted control of these currents will thus permit to control the power exchanged between the stator and the grid. If the stator flux is linked to the d-axis of the frame we have :

$$(13) \quad \psi_{ds} = \psi_s \quad \text{and} \quad \psi_{qs} = 0$$

and the electromagnetic torque can then be expressed as follows :

$$(14) \quad C_{em} = -pp\frac{M}{L_s}I_{qr}\psi_{ds}$$

By substituting Eq.13 in Eq.10, the following rotor flux equations are obtained :

$$(15) \quad \begin{cases} \psi_s = L_s I_{ds} + M I_{dr} \\ 0 = L_s I_{qs} + M I_{qr} \end{cases}$$

In addition, the stator voltage equations are reduced to :

$$(16) \quad \begin{cases} V_{ds} = R_s I_{ds} + \dfrac{d}{dt}\psi_s \\ V_{qs} = R_s I_{qs} + \omega_s\psi_s \end{cases}$$

By supposing that the electrical supply network is stable, having for simple voltage V_s, that led to a stator flux ψ_s constant. This consideration associated with Eq.14 shows that the electromagnetic torque only depends on the q-axis rotor current component. With these assumptions, the new stator voltage expressions can be written as follows :

$$(17) \quad \begin{cases} V_{ds} = R_s I_{ds} \\ V_{qs} = R_s I_{qs} + \omega_s\psi_s \end{cases}$$

Using Eq.15, a relation between the stator and rotor currents can be established :

$$(18) \quad \begin{cases} I_{ds} = -\dfrac{M}{L_s}I_{dr} + \dfrac{\psi_s}{L_s} \\ I_{qs} = -\dfrac{M}{L_s}I_{qr} \end{cases}$$

The stator active and reactive powers are written :

$$(19) \quad \begin{cases} P_s = V_{ds}I_{ds} + V_{qs}I_{qs} \\ Q_s = V_{qs}I_{ds} - V_{ds}I_{qs} \end{cases}$$

By using Eqs.9, 10, 17 and 18, the statoric active and reactive power, the rotoric fluxes and voltages can be written versus rotoric currents as :

$$(20) \quad \begin{cases} P_s = \dfrac{\omega_s\psi_s M}{L_s}I_{qr} - \dfrac{V_s^2}{R_s} + \dfrac{\omega_s^2\psi_s^2}{R_s} \\ Q_s = -\dfrac{\omega_s\psi_s M}{L_s}I_{dr} + \dfrac{\omega_s\psi_s^2}{L_s} \end{cases}$$

$$(21) \quad \begin{cases} \psi_{dr} = \left(L_r - \dfrac{M^2}{L_s}\right)I_{dr} + \dfrac{M\psi_s}{L_s} \\ \psi_{qr} = \left(L_r - \dfrac{M^2}{L_s}\right)I_{qr} \end{cases}$$

$$(22) \quad \begin{cases} V_{dr} = R_r I_{dr} + \left(L_r - \dfrac{M^2}{L_s}\right)\dfrac{dI_{dr}}{dt} - g\omega_s\left(L_r - \dfrac{M^2}{L_s}\right)I_{qr} \\ V_{qr} = R_r I_{qr} + \left(L_r - \dfrac{M^2}{L_s}\right)\dfrac{dI_{qr}}{dt} + g\omega_s\left(L_r - \dfrac{M^2}{L_s}\right)I_{dr} + g\omega_s\dfrac{M\psi_s}{L_s} \end{cases}$$

In steady state, the second derivative terms of the two equations in 22 are nil. We can thus write [14], [15]:

$$(23) \quad \begin{cases} V_{dr} = R_r I_{dr} - g\omega_s\left(L_r - \dfrac{M^2}{L_s}\right)I_{qr} \\ V_{qr} = R_r I_{qr} + g\omega_s\left(L_r - \dfrac{M^2}{L_s}\right)I_{dr} + g\omega_s\dfrac{M\psi_s}{L_s} \end{cases}$$

The third term, which constitutes cross-coupling terms, can be neglected because of their small influence. These terms can be compensated by an adequate synthesis of the regulators in the control loops. Based on the relations 18, 20 and 23, the control system can be designed in a cascade form, which is composed of two composed with two loops, an inner current loop and an outer power loop. Control systems are shown in Fig.3.

The blocks R_P and R_O represent active and reactive power regulators, while the blocks R_{Idr} and R_{Iqr} signify rotor currents regulators, respectively I_{dr} and I_{qr}. The aim of these regulators is to obtain high dynamic performances in terms of reference tracking, sensitivity to perturbations and robustness. To realize these objectives, Proportional Integral controller will be used. The synthesis of this controller is achieved by the classical method of pole compensation and will be detailed below.

PI regulator synthesis

This controller is simple to elaborate. Figure 4 shows the block diagram of the system implemented with this controller. The terms k_p and k_i represent respectively the proportional and integral gains. The quotient B/A represents the transfer function to be controlled, where A and B are presently defined as follows :

$$(24) \quad A = L_s R_r + s.L_s\left(L_r - \frac{M^2}{L_s}\right) \text{ and } B = \omega_s \psi_s M$$

The regulator terms are calculated with a pole-compensation method. The time response of the controlled system will be fixed at 10ms. This value is sufficient for our application and a lower value might involve transients with important overshoots. The calculated terms are :

$$(25) \quad k_i = \frac{1}{1\times10^{-3}}\frac{L_s R_r}{M\omega_s\psi_s}$$

$$(26) \quad k_p = \frac{1}{1\times10^{-3}}\frac{L_s(L_r - \frac{M^2}{L_s})}{M\omega_s\psi_s}$$
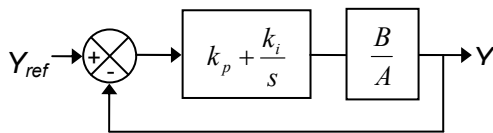
Fig.4. System with PI controller.

It is important to specify that the pole-compensation is not the only method to calculate a PI regulator but it is simple to elaborate with a first-order transfer-function and it is sufficient in our case to compare with other regulators. This synthesis method is also used to determine the current loops corrector's parameters. We can also note that the PI regulator presents several disadvantages :
- A zero is present in the numerator of the transfer-function,
- The integrator introduces a phase difference which can induce instability,
- The regulator is directly calculated with the parameters of the machine, if these parameters are varying, the robustness of the system can be affected,
- The eventual perturbations are not taken into account and the system has few degrees of freedom to be tuned.

Synoptic diagram

Figure 5 illustrates a general block diagram of the suggested DFIG control scheme. As shown in this figure, we can see that the stator of the machine is directly connected to the grid while the rotor is fed by a matrix converter controlled by the Venturini modulation technique. The errors between the rotor's currents references and those measured are treated by the control algorithm considered in order to conceive the rotor reference voltage standards. These reference voltage standards as those to the entry of the matrix converter are used by the modulation technique considered for synthesis of the control signals for the matrix converter bidirectional switches.
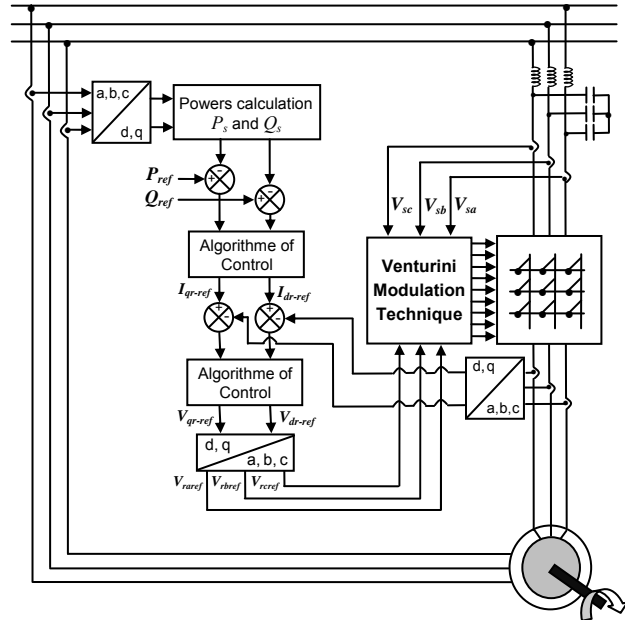
Fig.5. Schematic representation of the field-oriented controlled DFIG driven by a direct AC-AC converter.

Simulation results

In this part, simulations are investigated with a 5 kW generator connected to a 380V/50Hz grid. The machine's parameters are given next in appendix B. In this section, we are brought to represent all simulation results which enable to evaluate the performances brought by the control system considered for an operation at constant and variable speed.
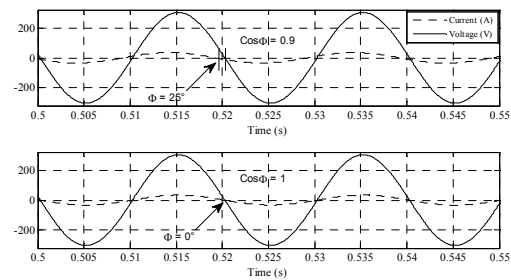
Fig.6. Power-factor control, grid side.

Power-factor control

The reference of the stator reactive power will be maintained null to ensure a unit power-factor in the stator side in order to optimize the energy quality returned on the network.

Figure 6 shows clearly the effectiveness of this method for the power-factor adjustment.

On the top figure : Q_{ref} = 2KVAr and P_{ref} = -5KW, whereas $cos\Phi$ is equal to 0.9, i.e a dephasing $\Phi = 25°$.On the bottom figure : Q_{ref} = 0KVAr and P_{ref} = -5KW, whereas $cos\Phi$ is unit, i.e a dephasing $\Phi = 0°$. We can thus compensate for the reactive power consumption of the

asynchronous machine and provide to the network a reactive power according to the request.
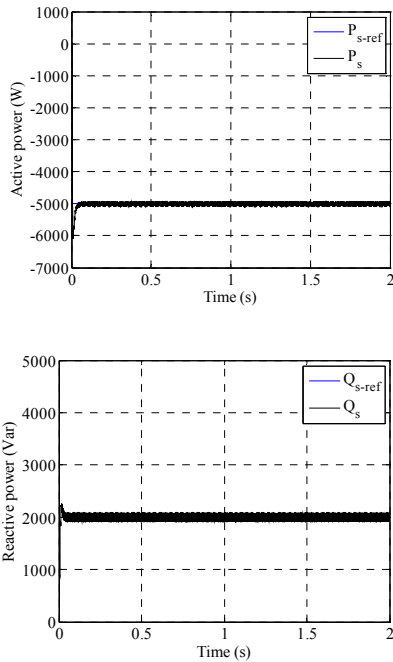
Fig.7. Stator active and reactive powers.

Reference tracking

The aim of this test is to analyze the reference tracking of the control system.

As it's shown in figure 7, it can be seen that the active and reactive generated powers tracks almost perfectly their references. In addition, in figure 8, it can be notice that the direct components of the stator current and the rotor current as well as the components into quadratic of these currents take the same forms, which reflects equation 10. In another side, figure 9 shows that currents obtained at the DFIG stator have sinusoidal form, which implies a clean energy without harmonics provided by the DFIG.
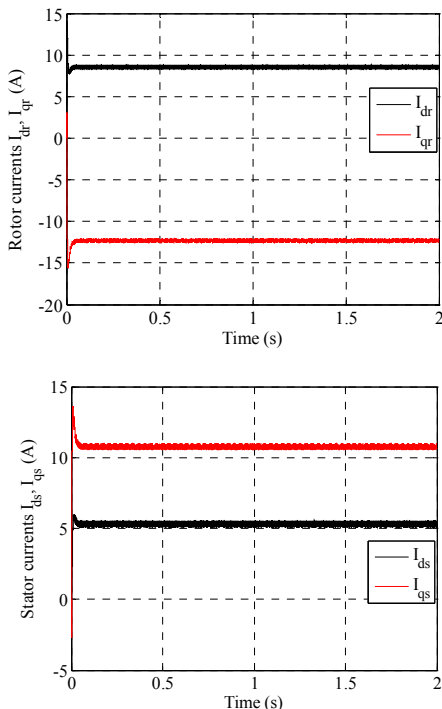
Fig.8. Two components of the stator and the rotor currents.

Figure 10 represent the wave forms of the simple voltage applied to the rotor circuit. This voltage is formed by crenels in which the widths are imposed by the venturini control algorithm.

As mentioned in paragraph (4.1), the PI controller has some disadvantages setting may affect its robustness against parameter variations.

To improve the performance of the control system and overcome the disadvantages of the PI controller, we used in the next section a different type of control known for its qualities of robustness, which is the sliding mode control.
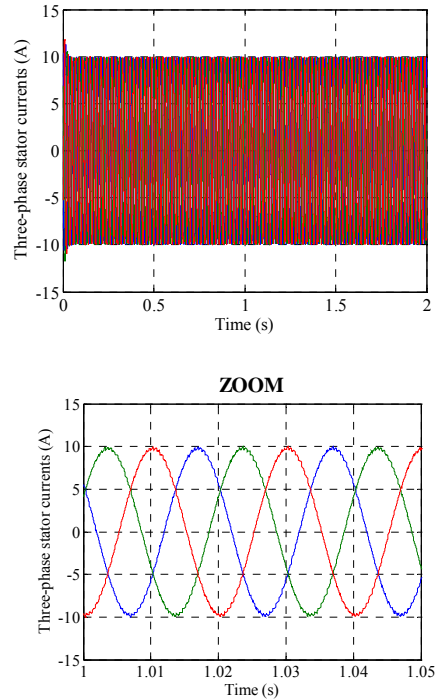
Fig.9. The three-phase stator currents.
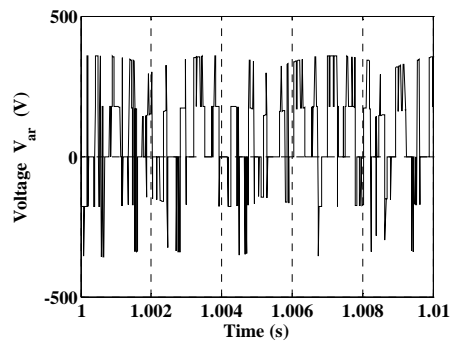
Fig.10. Rotor voltage versus time.

Sliding mode power control of DFIG
Design of the Sliding mode control

The sliding mode technique is developed from variable structure control (VSC) to solve the disadvantages of other designs of nonlinear control systems. The sliding mode is a technique to adjust feedback by previously defining a surface. The system which is controlled will be forced to that surface, then the behaviour of the system slides to the desired equilibrium point.

The main feature of this control is that we only need to drive the error to a "switching surface". When the system is in "sliding mode", the system behaviour is not affected by any modelling uncertainties and/or disturbances.

The design of the control system will be demonstrated for a nonlinear system presented in the canonical form [16,17,18] :

(27) $\dot{x} = f(x,t) + B(x,t)\,V(x,t)$, $x \in \Re^n$, $V \in \Re^m$, $\mathrm{ran}(B(x,t)) = m$

with control in the sliding mode, the goal is to keep the system motion on the manifold S, which is defined as :

(28) $$S = \{x : e(x,\,t) = 0\}$$

(29) $$e = x^d - x$$

Here e is the tracking error vector, x^d is the desired state vector, x is the state vector. The control input u has to guarantee that the motion of the system described in 10 is restricted to belong to the manifold S in the state space. The sliding mode control should be chosen such that the candidate Lyapunov function satisfies the Lyapunov stability criteria :

(30) $$\vartheta = \frac{1}{2} S(x)^2,$$

(31) $$\dot{\vartheta} = S(x)\dot{S}(x).$$

This can be assured for :

(32) $$\dot{\vartheta} = -\eta \left| S(x) \right|$$

Here η is strictly positive. Essentially, equation 30 states that the squared "distance" to the surface, measured by $e(x)^2$, decreases along all system trajectories. Therefore 31, 32 satisfy the Lyapunov condition. With selected Lyapunov function the stability of the whole control system is guaranteed. The control function will satisfy reaching conditions in the following form :

(33) $$V^{com} = V^{eq} + V^n$$

Here V^{com} is the control vector, V^{eq} is the equivalent control vector, V^n is the correction factor and must be calculated so that the stability conditions for the selected control are satisfied.

(34) $$V^n = K\,sat((S(x)/\delta)$$

$sat((S(x)/\delta)$ is the proposed saturation function, δ is the boundary layer thickness. In this paper we propose the Slotine method :

(35) $$S(X) = \left(\frac{d}{dt} + \lambda\right)^{n-1} e$$

Here, e is the tracking error vector, λ is a positive coefficient and n is the system order.

Active and reactive power control

The paper designs the following sliding mode, let :

(36) $$\begin{cases} S_1 = P_S^* - P_S \\ S_2 = Q_S^* - Q_S \end{cases}$$

Where P^* and Q^* are the expected active power and reactive power reference.
The first order derivate of 36, gives :

(37) $$\begin{cases} \dot{S}_1 = \dot{P}_S^* - \dot{P}_S \\ \dot{S}_2 = \dot{Q}_S^* - \dot{Q}_S \end{cases}$$

Replacing the expression of the power by their expressions given in 20, the equations below are expressed :

(38) $$\begin{cases} \dot{S}_1 = \dot{P}_S^* - \dfrac{\omega_s \psi_s M}{L_s}\dot{I}_{qr} + \dfrac{V_s^2}{R_s} - \dfrac{\omega_s^2 \psi_s^2}{R_s} \\ \dot{S}_2 = \dot{Q}_S^* + \dfrac{\omega_s \psi_s M}{L_s}\dot{I}_{dr} - \dfrac{\omega_s \psi_s^2}{L_s} \end{cases}$$

It takes the current expression of $\dot{I}_{dr}$ and $\dot{I}_{qr}$, with the voltage equation 23 and taking into consideration the sliding mode in the steady state ($S=0$, $\dot{S}=0$).
The equivalent control vector V^{eq} can expressed by :

(39)
$$\begin{cases} V_{dr}^{eq} = -\dfrac{L_s\left(L_r - \dfrac{M^2}{L_s}\right)}{\omega_s \psi_s M}\dot{Q}_s^* + R_r I_{dr} - \left(L_r - \dfrac{M^2}{L_s}\right)g\omega_s I_{qr} + \dfrac{\left(L_r - \dfrac{M^2}{L_s}\right)\psi_s}{M} \\[4ex] V_{qr}^{eq} = \dfrac{L_s}{\omega_s \psi_s M}\dot{P}_s^* + R_r I_{qr} - \left(L_r - \dfrac{M^2}{L_s}\right)g\omega_s I_{dr} + \dfrac{g\omega_s \psi_s M}{L_s} + \dfrac{L_s(V_s^2 - \omega_s^2 \psi_s^2)}{\omega_s \psi_s M R_s} \end{cases}$$

In our case, we have : $V = V^{eq} + V^n$
V^n is the saturation function defined by : $V^n = -K.sat(S)$.
where K determine the ability of overcoming the chattering.

Simulation results and discussions

The block diagram of the proposed robust control scheme is presented in figure 11. The blocks SMC1, SMC2, are sliding mode controllers which represent, respectively, active and reactive power controllers. The DFIG is fed by a matrix converter. The global system is simulated in real time by the software Matlab/Simulink.

The first test is investigated to compare the reference tracking of the two types of control (field oriented control with PI regulators and sliding mode control), while the machine's speed is maintained constant at its nominal value. The machine is considered as working over ideal conditions (no perturbations and no parameters variations). The simulation results are presented in figures 12-13. As it's shown in figure 12, it can be seen that for the two types of control used, the active and reactive generated powers tracks almost perfectly their references. In addition and contrary to PI regulator where the coupling effect between the two axes (appear on active and reactive powers) is very clear, we can notice that the sliding mode control ensures a perfect decoupling between them. In the other hand and as it shown in figure 13, is very clear that the stator current delivered by the DFIG controlled by sliding mode controller is less disturbed than that delivered by the DFIG controlled by PI regulators. Therefore we can consider that the sliding mode controller has a very good behaviour for this test.

Robustness tests

The aim of these tests is to analyze the influence of the DFIG's parameters variations on the controllers' performances. The DFIG is running at its nominal speed, the obtained results are presented in figures 14-15.

In the first test, the stator resistance value is doubled to examine the influence of its variation on the controllers' behavior. This is carried out only for extracting the importance of this parameter in the machine model. As it's shown in figure 14, variation of this resistance present a slightly considerable effect especially appear in errors curves of the two powers, particularly in their high values. This result makes it possible to justify our choice to use the real model of the machine without neglecting this resistance.

In the second test, we examined the influence of all the DFIG's parameters variations on the controller's performances. For that, the machines' model parameters have been deliberately modified with excessive variations: the values of the stator and the rotor resistances R_s and R_r are doubled and the values of inductances L_s, L_r and M are divided by 2, the obtained results are presented in figure 14.

These results show that parameters variations of the DFIG increase the time-response of the PI but not the sliding mode controller's one. The transient oscillations due to the coupling terms between the two axes are always

present for PI controllers. However, and as it is shown by the curves of errors, we notice that this variation presents an observable effect on these curves and that the effect proves more significant for PI controller than that with sliding mode controller's one. This result enables us to conclude that this control type is more robust.
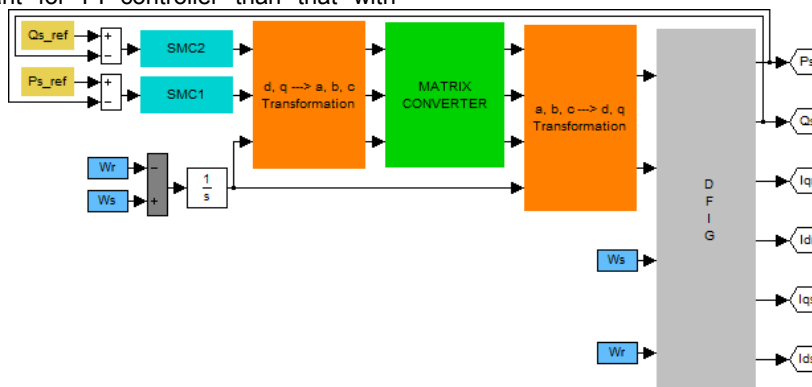
Fig.11. Block diagram of the proposed robust control scheme of DFIG.
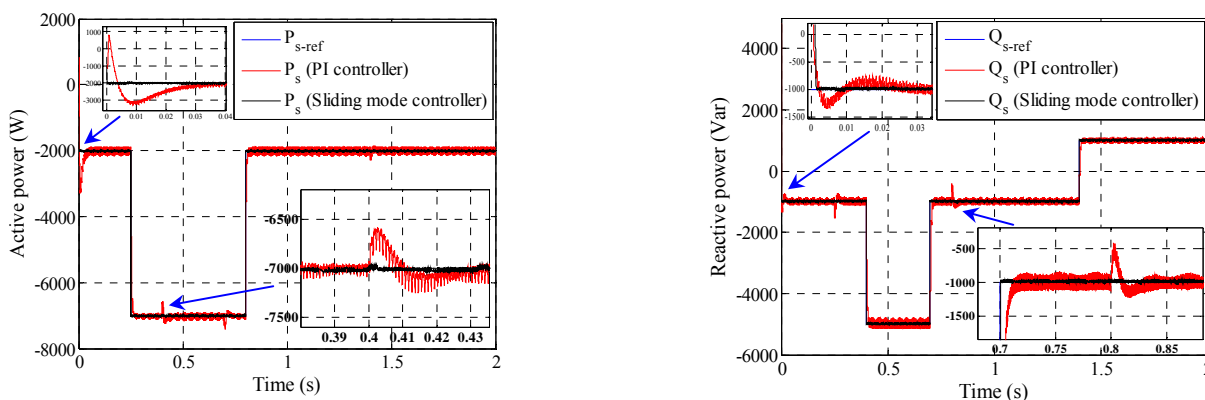
Fig.12. Stator active and reactive powers.
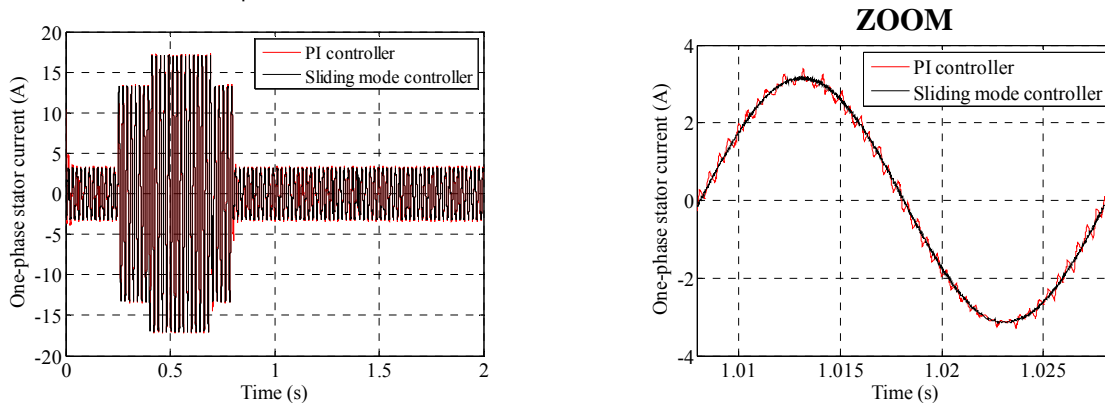
Fig.13. One-phase stator current.
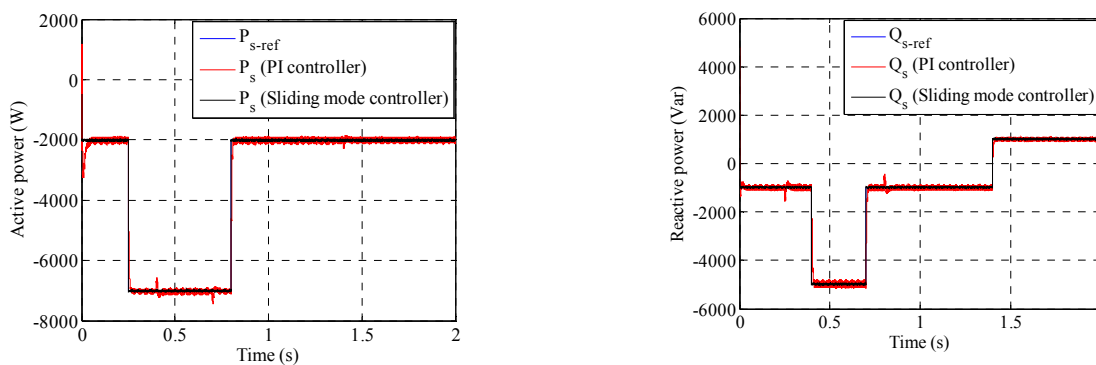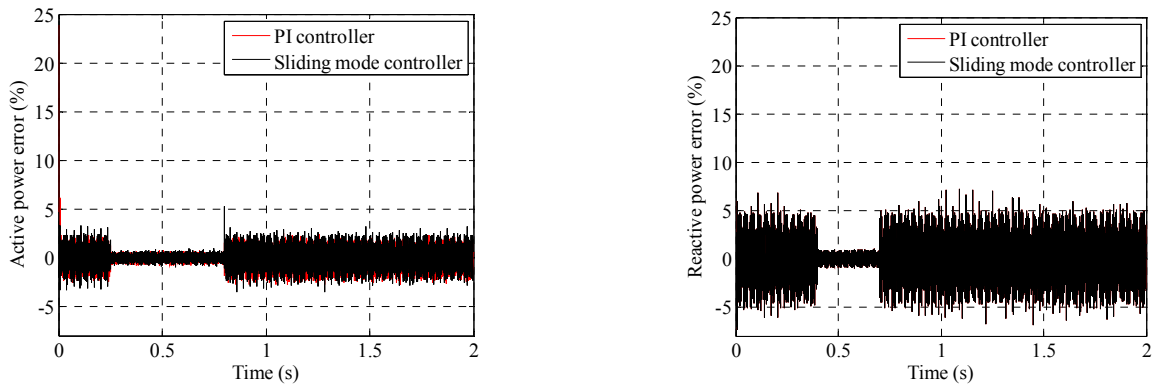
Fig.14. Effect of the stator resistance variation on the robust control of the DFIG.
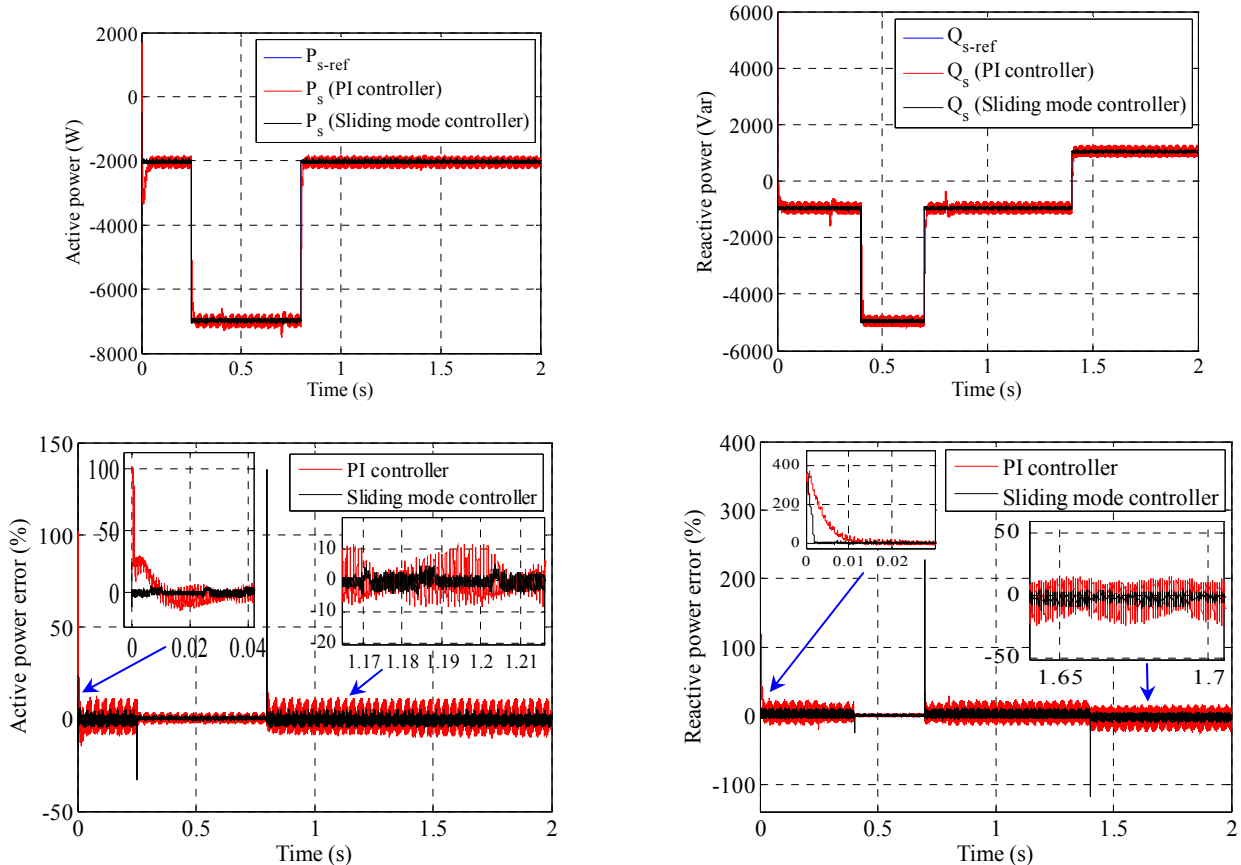
Fig.15. Effect of all machine's parameters variation on the robust control of the DFIG.

Conclusion

The modeling, the control and the simulation of an electrical power electromechanical conversion system based on the doubly fed induction generator connected directly to the grid by the stator and fed by a matrix converter on the rotor side has been presented in this study. Our objective was the implementation of a robust decoupled control system of active and reactive powers generated by the stator side of the DFIG, in order to ensure of the high performance and a better execution of the DFIG, and to make the system insensible with the external disturbances and the parametric variations. In the first step, we started with a study of modeling on the matrix converter controlled by the venturini modulation technique, because this later present a reduced harmonic rate and the possibility of operation of the converter at the input unit power factor. In second step, we adopted a vector control strategy in order to control statoric active and reactive

power exchanged between the DFIG and the grid. Contrary to the previous work carried out on the DFIG where the researchers always neglect the stator resistance to facilitate its control, in our work this resistance was not neglected in order to return the system studied near to reality. In third step and in order to improve the performances of the control device, PI regulators were removed and substituted by others of sliding mode type. Simulation results have shown that the sliding mode control ensures a perfect decoupling between the two axes comparatively to PI regulators where the coupling effect between them is very clear. They also showed that the sliding mode controllers are more robust under parameters variations of the DFIG.

Appendix A. Machine parameters

Parameters	Rated Values	Unity
Nominal power	5	KW
Stator voltage	380	V
Stator frequency	50	Hz

Number of pairs poles	3	
Nominal speed	100	rad/s
Stator resistance	0.95	Ω
Rotor resistance	1.8	Ω
Stator inductance	0.094	H
Rotor inductance	0.088	H
Mutual inductance	0.082	H
Inertia	0.1	Kg.m^2

Appendix B. List of symbols

Symbol	Significance
$V_{ds}, V_{qs}, V_{dr}, V_{qr}$	Two-phase stator and rotor voltages,
$\psi_{ds}, \psi_{qs}, \psi_{dr}, \psi_{qr}$	Two-phase stator and rotor fluxes,
$I_{ds}, I_{qs}, I_{dr}, I_{qr}$	Two-phase stator and rotor currents,
R_s, R_r	Per phase stator and rotor resistances,
L_s, L_r	Per phase stator and rotor inductances,
M	Mutual inductance,
p	Number of pole pairs,
s	Laplace operator,
ω_s, ω_r	Stator and rotor currents frequencies (rad/s),
ω	Mechanical rotor frequency (rad/s),
P_s, Q_s	Active and reactive stator power,
J	Inertia,
f	Coefficient of viscous frictions,
C_r	Load torque,
C_{em}	Electromagnetic torque.

REFERENCES

[1] Anaya-Lara O., Jenkins N., Ekanayake J., Cartwright P. and Hughes M., Wind Energy Generation, *Wiley*, (2009).
[2] Venturini M., A new sine wave in sine wave out conversion technique which eliminates reactive elements, In: Proc Powercon 7, San Diego, CA, pp E3-1, E3-15, 27-24 March 1980.
[3] Alesina A., Venturini M., Solid-state power conversion: a Fourier analysis approach to generalized transformer synthesis, *IEEE T Circuits Syst* 28: 319-330, (1981).
[4] Pena R., Clare J.C., Asher G.M., A doubly fed induction generator using back to back converters supplying an isolated load from a variable speed wind turbine, *IEE Proceeding on Electrical Power Applications 143* (September (5)) (1996).
[5] Poller M.A., Doubly-fed induction machine models for stability assessment of wind farms, in: Power Tech Conference Proceedings, 2003, *IEEE, Bologna*, vol. 3, 23–26 June 2003.
[6] Brekken T., Mohan N., A novel doubly-fed induction wind generator control scheme for reactive power control and torque pulsation compensation under unbalanced grid voltage conditions, in: *IEEE 34th Annual Power Electronics Specialist Conference*, 2003, PESC '03, 15–19 June 2003, vol. 2, pp. 760–764.
[7] Brekken T.K.A., Mohan N., Control of a doubly fed induction wind generator under unbalanced grid voltage conditions, *IEEE Transaction on Energy Conversion* 22 (March (1)) (2007) 129–135.
[8] Lopez J., Sanchis P., Roboam X., Marroyo L., Dynamic behavior of the doubly fed induction generator during three-phase voltage dips, *IEEE Transaction on Energy Conversion* 22 (September (3)) (2007) 709–717.
[9] Sun T., Chen Z., Blaabjerg F., Flicker study on variable speed wind turbines with doubly fed induction generators, *IEEE Transactions on Energy Conversion* 20 (December (4)) (2005) 896–905.
[10] Piegari L., Rizzo R., A control technique for doubly fed induction generators to solve flicker problems in wind power generation, in: *International Power and Energy Conference*, Putrajaya, Malaysia, 28 and 29 November 2006, pp. 19–23.
[11] Sünter S., A vector controlled matrix converter induction motor drive, PhD Thesis, University of Nottingham, Nottingham, UK, (1995).
[12] Ghedamsi K., Aouzellag D. and Berkouk E. M., Matrix converter based variable speed wind generator system, International Journal of Electrical and Power Engineering 2 (1), 39-49, (2008).
[13] Amari A., Nonlinear control of a doubly fed induction generator for wind energy conversion systems, PG1 Thesis, University of Mostaganem, Algiers (2011).
[14] Poitier F., Study and control of induction generators for wind energy conversion systems, PhD Thesis, University of Nantes, (2003).
[15] Boyette A., Control of a doubly fed asynchronous generator with a storage system for the wind production, PhD Thesis, University of Nancy 1, (2006).
[16] Utkin V. I., Variable Structure Systems with Sliding Modes, IEEE Trans. Automat. contr, AC-22 (February 1993), 212–221.
[17] Yan Z., Jin C., Utkin V. I., Sensorless Sliding-Mode Control of Induction Motors, IEEE Trans. Ind. electronic. 47 No. 6 (December 2000), 1286–1297.
[18] Abid M., Ramdani Y., Meroufel A., Speed sliding mode control of sensorless induction machine, JEE, Vol. 57, N°1, 2006, 47-51.

Authors : Zinelaabidine BOUDJEMA, PhD student, Intelligent Control & Electrical Power Systems Laboratory, Faculty of Engineer Science, Electrical Engineering Department, University of Djillali Liabes, BP 98 Sidi Bel-Abbès 22000 Algeria, E-mail: boudjemaa1983@yahoo.fr; Professor Abdelkader MEROUFEL, Intelligent Control & Electrical Power Systems Laboratory, Faculty of Engineer Science, Electrical Engineering Department, University of Djillali Liabes, BP 98 Sidi Bel-Abbès 22000 Algeria, E-mail: ameroufel@yahoo.fr; Ahmed AMARI, PhD student, Electrical Engineering Department, University of Mostaganem E-mail: amariahmed39@yahoo.fr.